



# Characterization of the *Vibrio cholerae* extracellular matrix: A top-down solid-state NMR approach<sup>☆</sup>



Courtney Reichhardt<sup>a</sup>, Jiunn C.N. Fong<sup>b</sup>, Fitnat Yildiz<sup>b</sup>, Lynette Cegelski<sup>a,\*</sup>

<sup>a</sup> Department of Chemistry, Stanford University, Mudd Building, Room 121, 333 Campus Drive, Stanford, CA 94305, USA

<sup>b</sup> Department of Microbiology and Environmental Toxicology, UC Santa Cruz, 1156 High Street, Santa Cruz, CA 95064, USA

## ARTICLE INFO

### Article history:

Received 14 May 2014

Received in revised form 30 May 2014

Accepted 30 May 2014

Available online 7 June 2014

### Keywords:

*Vibrio cholerae*

Biofilm

Solid-state NMR

CPMAS

REDOR

Extracellular matrix (ECM)

## ABSTRACT

Bacterial biofilms are communities of bacterial cells surrounded by a self-secreted extracellular matrix. Biofilm formation by *Vibrio cholerae*, the human pathogen responsible for cholera, contributes to its environmental survival and infectivity. Important genetic and molecular requirements have been identified for *V. cholerae* biofilm formation, yet a compositional accounting of these parts in the intact biofilm or extracellular matrix has not been described. As insoluble and non-crystalline assemblies, determinations of biofilm composition pose a challenge to conventional biochemical and biophysical analyses. The *V. cholerae* extracellular matrix composition is particularly complex with several proteins, complex polysaccharides, and other biomolecules having been identified as matrix parts. We developed a new top-down solid-state NMR approach to spectroscopically assign and quantify the carbon pools of the intact *V. cholerae* extracellular matrix using <sup>13</sup>C CPMAS and <sup>13</sup>C {<sup>15</sup>N}, <sup>15</sup>N {<sup>31</sup>P}, and <sup>13</sup>C {<sup>31</sup>P} REDOR. General sugar, lipid, and amino acid pools were first profiled and then further annotated and quantified as specific carbon types, including carbonyls, amides, glycol carbons, and anomers. In addition, <sup>15</sup>N profiling revealed a large amine pool relative to amide contributions, reflecting the prevalence of molecular modifications with free amine groups. Our top-down approach could be implemented immediately to examine the extracellular matrix from mutant strains that might alter polysaccharide production or lipid release beyond the cell surface; or to monitor changes that may accompany environmental variations and stressors such as altered nutrient composition, oxidative stress or antibiotics. More generally, our analysis has demonstrated that solid-state NMR is a valuable tool to characterize complex biofilm systems. This article is part of a Special Issue entitled: NMR Spectroscopy for Atomistic Views of Biomembranes and Cell Surfaces. Guest Editors: Lynette Cegelski and David P. Weliky.

© 2014 Published by Elsevier B.V.

## 1. Introduction

Bacteria associate with surfaces and one another by elaborating an extracellular matrix (ECM) to encapsulate and connect cells, creating communities termed biofilms. The self-secreted ECM can include polysaccharides and proteins as well as lipids, DNA, and other small molecules. Biofilms provide protection from physical external stresses such as desiccation and shear flow, and from chemical stresses such as antibiotics and host defenses [1–4]. In this way, biofilms are implicated in bacterial persistence in the environment. They enhance bacteria survival during growth on inanimate surfaces in hospitals and food processing plants, in aquatic environments such as ship hulls [5], and in high shear force environments [2] that include interfaces with contact lenses [6] and heart valve replacements [7]. In the human host, biofilms often

confer resistance to antibiotics and contribute to serious and chronic infectious diseases including recurrent urinary tract infections [8–11] and cystic fibrosis pneumonia [12]. The bacterium investigated in this study, *Vibrio cholerae*, is the pathogen responsible for the illness cholera [13]. Its biofilm contributes to its environmental survival as it provides increased resistance against osmotic and oxidative stress as well as protection against predation by protozoa and phages [14,15]. Biofilm formation is also implicated in the infectivity of *V. cholerae* and is involved in seasonal outbreaks of cholera [16,17].

Intact biofilms are both insoluble and non-crystalline, which poses a challenge to analysis by most biochemical and biophysical techniques [18]. The same is true for extracted preparations of extracellular matrix material. As such, descriptions of the composition of the ECM of different bacteria are often not complete. They are usually generated from various treatments of the ECM including harsh acid hydrolysis and enzymatic digests followed by various precipitation protocols in attempts to separate and collect distinct components such as the protein and polysaccharide portions. The apparent contributions of polysaccharides and proteins to the overall ECM composition can vary widely and depend upon the extraction and analysis methods [18]. Ideally, analysis

<sup>☆</sup> This article is part of a Special Issue entitled: NMR Spectroscopy for Atomistic Views of Biomembranes and Cell Surfaces. Guest Editors: Lynette Cegelski and David P. Weliky.

\* Corresponding author. Tel.: +1 650 725 3527.

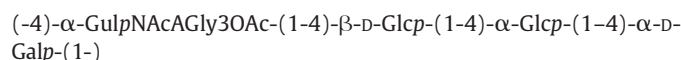
E-mail addresses: [creich@stanford.edu](mailto:creich@stanford.edu) (C. Reichhardt), [jiunn@ucsc.edu](mailto:jiunn@ucsc.edu) (J.C.N. Fong), [fyildiz@ucsc.edu](mailto:fyildiz@ucsc.edu) (F. Yildiz), [cegelski@stanford.edu](mailto:cegelski@stanford.edu) (L. Cegelski).

of intact biofilms and the ECM should be performed holistically without preliminary treatment or degradation, thus preventing loss and subsequent misrepresentation of matrix composition [19,20].

We recently developed an approach to define the composition of intact ECM integrating solid-state NMR with electron microscopy and biochemical analysis [19]. Solid-state NMR is uniquely suited to examine such complex, insoluble networks, ranging from bacterial cell walls [21,22] and ECM [19] to insect cuticle [23] and intact plant leaves [24], because it can provide quantitative information about chemical composition, connectivity, and spatial contacts of components without requiring perturbative sample preparation. In work with *Escherichia coli*, we provided a complete sum-of-the-parts accounting of the insoluble ECM formed by UT189, a clinically relevant, uropathogenic strain of *E. coli* that forms robust amyloid-integrated biofilms when grown on YESCA nutrient agar that are characterized by the hallmark wrinkled colony morphology exhibited by many bacterial biofilm formers. We determined that the insoluble ECM was composed of two major components by mass: curli amyloid fibers (85%) and a modified form of cellulose (15%).  $^{13}\text{C}$  cross-polarization magic-angle spinning (CPMAS) NMR spectra were obtained for the intact ECM and of the two separate parts, purified curli and purified polysaccharide. Although not expected, a simple scaled sum of the two parts was able to entirely recapitulate the spectrum of the intact ECM, which was further confirmed by a physical mixture of curli plus polysaccharide in the calculated ratio of 6:1. This was the first quantification of the components of intact ECM and illustrated the power of solid-state NMR to examine bacterial ECM composition using solid-state NMR [19].

In this study, we have applied solid-state NMR to characterize the more complex biofilm system of *V. cholerae* (using the O1 El Tor rugose variant, A1552R). Unlike the *E. coli* system described above, we did not have purified samples of major matrix components. Thus, we developed a new top-down approach to dissect the *V. cholerae* ECM using  $^{13}\text{C}$  CPMAS and  $^{13}\text{C}\{^{15}\text{N}\}$  and  $^{13}\text{C}\{^{31}\text{P}\}$ REDOR in order to investigate, assign, and quantify the ECM carbon pools.

As with many biofilms, some genetic and molecular determinants, as well as a kind of biofilm parts lists, have been identified for our rugose strain of *V. cholerae*. In particular, *V. cholerae* biofilm production requires the production of *Vibrio* exopolysaccharide (VPS) [25]. Compositional analysis of extracted, solubilized, and further digested polysaccharide fractions of the ECM identified glucose and galactose as well as lower levels of glucosamine as contributing to the polysaccharide building blocks [26]. Recent structural analysis of VPS using solution-state NMR identified the main component (80%) of VPS that was able to be solubilized as:



where  $\alpha\text{-D-Glc}$  is partially replaced (20%) with  $\alpha\text{-D-GlcNAc}$  [27]. This work provided a valuable description of one of the necessary components of *V. cholerae* ECM. However, harsh processing of the intact ECM was required to remove proteins and other components and to lower the viscosity for improving NMR signal of the more soluble components and, thus, does not provide a complete accounting of the VPS. Individual proteins also contribute to biofilm phenotypes including Bap1, RbmA, and RbmC [25,28], yet determining the overall relative compositional contributions of matrix parts within the intact ECM presents a challenge to methods that ultimately require soluble components. In addition, lipopolysaccharide (LPS) contributes to the formation of outer membrane vesicles (OMVs) that are found beyond the cell surface and may be present in ECM preparations [29–31]. In our work presented here, we aimed to provide a complete accounting of the ECM carbon pools and the chemical building blocks (e.g. amino acids, lipid carbonyls, sugar carbons) using selective and quantitative solid-state NMR measurements involving  $^{13}\text{C}$ ,  $^{15}\text{N}$ , and  $^{31}\text{P}$  nuclei on ECM prepared with minimal perturbation from *V. cholerae* grown on a minimal nutrient agar

medium with uniform  $^{15}\text{N}$  labeling. Our analysis helps place VPS and other ECM components into the greater compositional context of the intact *V. cholerae* biofilm.

## 2. Materials and methods

### 2.1. Bacterial strains, growth conditions, and ECM extraction

Bacterial growth and ECM isolation were carried out similar to a previous published protocol [27]. Briefly, *V. cholerae* rugose variant, A1152R, was grown overnight aerobically in Luria-Bertani (LB) medium at 30 °C. An overnight-grown culture (500  $\mu\text{L}$ ) was plated onto cellulose dialysis membranes placed on the surface of uniformly  $^{15}\text{N}$ -enriched M9 medium agar plates (150  $\times$  15 mm) supplemented with MEM vitamin solution and glucose (10 mM) and incubated for 48 h at 30 °C. Bacteria were harvested from 100 plates, suspended in 400 mL of ice-cold 10 mM Tris buffer, and shaken on a rotary shaker for 24 h at 4 °C, which serves to separate the ECM from the bacterial cell surface. The bacteria cells were removed by centrifugation twice for 30 min at 5000 g, 4 °C, followed by an additional centrifugation step of 30 min at 9000 g to ensure complete removal of bacterial cells. The resulting supernatant was dialyzed against distilled water containing 0.02% sodium azide for 2 days. The supernatant was frozen and lyophilized.

The agar colony morphology assay was initiated by dropping 10  $\mu\text{L}$  of an overnight bacterial culture grown at 37 °C onto minimal agar medium and incubated at 30 °C for 48 hours.

### 2.2. Electron microscopy

Negative staining transmission electron microscopy was performed on ECM samples that were applied to 300-mesh copper grids coated with Formvar film (Electron Microscopy Sciences, Hatfield, PA) for 2 min, rinsed in deionized water. The samples were negatively stained with 2% uranyl acetate for 90 s and then air-dried. Microscopy was performed on the JEM-1400 (JEOL, LLC). Scanning electron microscopy was performed on an intact bacterial biofilm grown on minimal nutrient agar medium, cut in an intact agar block and prepared as follows: fixed in 2% glutaraldehyde/4% formaldehyde in 0.1 M sodium cacodylate buffer (pH 7.3) in a Petri dish for 45 min at 4 °C, washed and then postfixed with 1% osmium tetroxide in 0.1 M sodium cacodylate buffer for 45 min. The fixed biofilm sample was dehydrated in a series of increasing concentrations of ethanol (50%, 70%, 95%, and 100%), inserted into a critical point dryer (CPD) to remove residual ethanol with carbon dioxide, and then coated with gold–palladium and visualized with a Hitachi S-3400N scanning electron microscope.

### 2.3. SDS-PAGE protein analysis

Lyophilized ECM was resuspended in water to give a final concentration of 1 mg/mL. Resuspended ECM aliquots containing 1.5  $\mu\text{g}$ , 15  $\mu\text{g}$ , and 150  $\mu\text{g}$  of sample were frozen and lyophilized again. The lyophilized aliquots were resuspended in 100  $\mu\text{L}$  of 88% formic acid and vacuum centrifuged until dry. The samples were reconstituted in SDS-PAGE sample buffer containing 8 M urea and 50 mM DTT and used for electrophoresis.

### 2.4. Solid-state NMR

All solid-state NMR experiments were performed using an 89-mm wide-bore Varian magnet at 11.7 T (499.12 MHz for  $^1\text{H}$ , 125.52 MHz for  $^{13}\text{C}$ , and 50.58 MHz for  $^{15}\text{N}$ ) and an 89-mm wide-bore Agilent magnet at 11.7 T (500.92 MHz for  $^1\text{H}$ , 125.97 MHz for  $^{13}\text{C}$ , 50.76 MHz for  $^{15}\text{N}$ , and 202.78 MHz for  $^{31}\text{P}$ ), Varian/Agilent consoles, and home-built four-frequency transmission-line probes with a 13.66 mm long, 6 mm inner-diameter sample coil and a Revolution NMR MAS Vespel stator. Samples were spun in thin-wall 5 mm outer-diameter zirconia

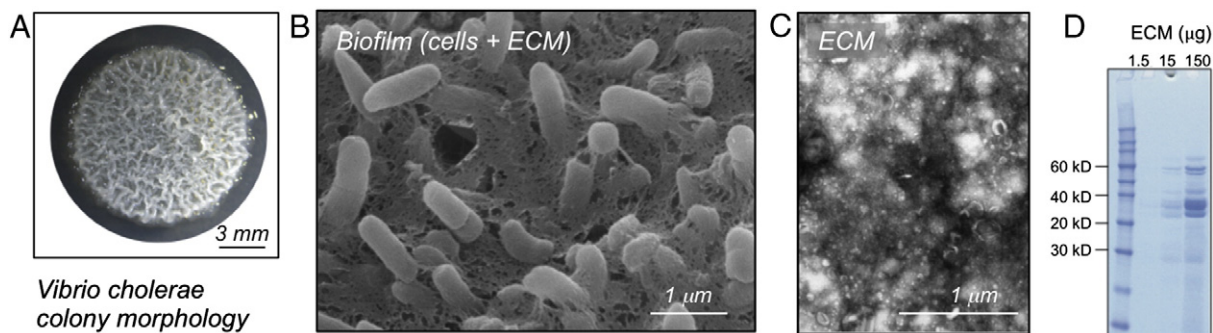


**Fig. 1.** *V. cholerae* biofilm and extracted ECM. (A) *V. cholerae* forms rugose, or wrinkled colonies, indicative of biofilm formation. (B) Scanning electron micrograph of *V. cholerae* biofilm (cells plus ECM). (C) Transmission electron micrograph of isolated *V. cholerae* ECM reveals amorphous aggregates and vesicles. (D) SDS-PAGE protein gel of the *V. cholerae* ECM contains bands corresponding to seven different proteins.

rotors (Revolution NMR, LLC) at  $7143 \pm 2$  Hz, using a Varian MAS control unit. The temperature was maintained at  $-10$  °C. For all NMR experiments,  $\pi$ -pulse lengths were  $7 \mu\text{s}$  for  $^1\text{H}$  and  $10 \mu\text{s}$  for  $^{13}\text{C}$ ,  $^{15}\text{N}$ , and  $^{31}\text{P}$ . Proton–carbon and proton–nitrogen cross-polarization occurred at 50 kHz for 1.5 ms unless otherwise noted. Proton dipolar coupling was performed at 90 kHz with TPPM modulation. For all experiments, the recycle delay was 3 s. The chemical shift of  $^{13}\text{C}$  spectra was referenced to external adamantane, and  $^{15}\text{N}$  spectra were referenced externally to liquid ammonia. REDOR dephasing was calculated using peak integral values. Multi-peak fitting and integration were performed in software written for Igor Pro (WaveMetrics, Lake Oswego, OR, USA).

### 3. Results and discussion

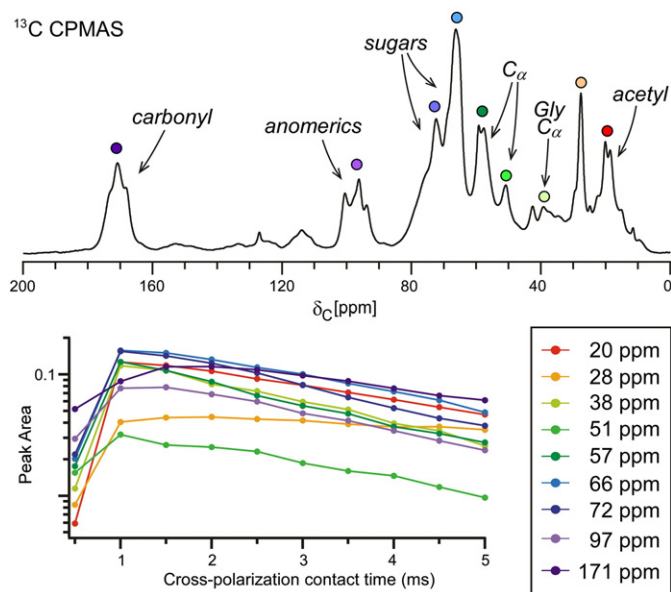
#### 3.1. $^{13}\text{C}$ CPMAS provides an overview of *V. cholerae* ECM carbon pools

A biofilm contains both bacterial cells and ECM. To examine the composition of the ECM separately from the intracellular components of the bacteria, we extracted the ECM using a minimally perturbative method based on a previous crude VPS extraction protocol. The ECM was extracted from the *V. cholerae* O1 El Tor rugose variant, A1552R, which forms wrinkled colonies indicative of high VPS production and biofilm formation (Fig. 1A). The community of cells plus the ECM can be appreciated in more detail through visualization of the biofilm by scanning electron microscopy (Fig. 1B). Transmission electron microscopy is better suited to examine the isolated ECM material and revealed aggregative material combined with vesicle-type structures (Fig. 1C). SDS-PAGE analysis of the ECM revealed bands corresponding to seven proteins of different molecular weights (Fig. 1D). ECM samples are treated with formic acid in order to increase the amount of soluble proteins that will run into the gel, yet some insoluble material still remained in the loading well even after formic acid treatment, making it impossible to quantify exactly how much protein was in the ECM. Yet, a lower limit was determined by the amount of protein that was detected. Comparison of the protein band intensities to a bovine serum albumin standard showed that proteins contribute to at least 1–2% of the ECM dry mass. To extract more quantitative detail, we implemented a solid-state NMR approach that does not depend upon sample solubility to examine the intact material.

The  $^{13}\text{C}$  cross-polarization magic-angle spinning (CPMAS) NMR spectrum [32] (Fig. 2) demonstrated that the ECM is a complex mixture with carbon chemical shifts that are consistent with proteins (carbonyl, 171 ppm;  $\alpha$ -carbons, 51–58 ppm; other aliphatics 10–40 ppm), polysaccharides (anomeric carbons, 94–100 ppm; ring-sugar carbons 60–80 ppm), glycine ( $\alpha$ -carbons, 38–43 ppm), acetyl modifications (20–22 ppm), lipids (20, 38, and 171 ppm), and possibly DNA.

CPMAS spectra can preferentially represent rigid or protonated chemical sites over mobile or unsaturated sites. For CPMAS to be

used quantitatively to report on the number of spins at corresponding chemical shifts relative to others in a spectrum, one must account for any differences that might be present in cross-polarization behavior of different spin types. We obtained CP buildup curves (Fig. 2) and determined the quantitative contributions of each distinguishable peak in the spectrum (Figure S1) by extrapolation. The anomeric carbons from sugars contribute uniquely to the 94–100 ppm region of the spectrum and account for 8–9% of the total carbon. The peaks consistent with ring sugars (66 and 72 ppm) are dominant spectral features and account for 31–34% of the carbon pool, given the details of the extrapolation (Table 1). These results are consistent with sugar structures containing four other ring carbons in addition to the anomeric carbon. Together, these results suggest that *V. cholerae* ECM is sugar rich. The high sugar content of *V. cholerae* ECM is in contrast to the UTI89 *E. coli* ECM, which is primarily protein [19]. This result highlights the differences between biofilms formed by different species and the importance of a quantitative approach when studying biofilms.

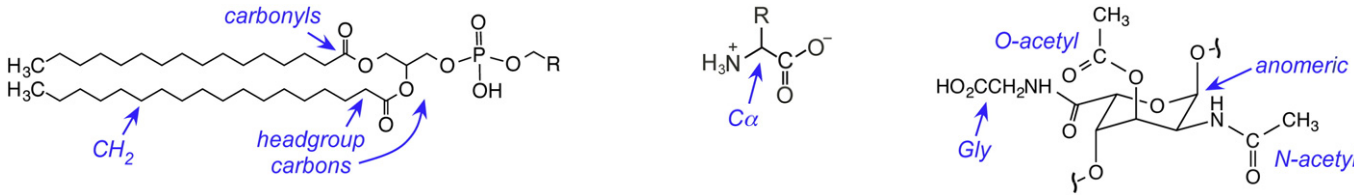


**Fig. 2.** ECM carbon pools by CPMAS. (Top) The  $^{13}\text{C}$  CPMAS spectrum of *V. cholerae* ECM includes notable contributions from proteins, lipids, and polysaccharides (56,600 scans). (Bottom) CPMAS spectra were obtained as a function of CP time to obtain absolute carbon contributions (1640 scans each).



**Table 1**

Defined carbon pools of *V. cholerae* ECM. Unique carbon types were identified and quantified using CPMAS and REDOR NMR, and accounted specifically for 82% of the total carbon. An additional 18% of the carbon mass is distributed amongst peaks between 130–160 ppm, 50–60 ppm, 38–43 ppm, and 10–25 ppm, and is ascribed to amino acid side chain carbons and phospholipid components that were not uniquely assigned. The “modified sugar” is  $\alpha$ -GulPNAcAGly<sub>3</sub>OAc as found in VPS [27]. \*The percent of total carbon mass was determined by extrapolation of the CP curves. CP curves for peaks from 60 to 80 ppm (centered at 57, 66, and 72 ppm) exhibited nonlinear behavior, and extrapolations to fit multiple components varied between 31 and 34%.

Chemical shift, $^{13}\text{C}$	171 ppm	94–100 ppm	60–80 ppm	50–60 ppm	38–43 ppm	25–30 ppm	10–25 ppm
Carbon type	Carbonyls	Anomerics	Ring carbons	Other $\text{C}_\alpha$ and sugar C–N	Gly $\text{C}_\alpha$	$\text{CH}_2\text{s}$	C–X–N aliphatics
Carbon mass (% of total)	16%	9%	34%	6%	4%	6%	7%
Molecules	Amino acids, phospholipids, N- and O-acetyl modifications	Sugars	Sugars	Amino acids, N-modified sugars	Gly (proteins and polysaccharide modifications)	Phospholipids, amino acids	Amino acids, acetyl modifications
Representative chemical structures							
							
	Phospholipids		Amino acids		Modified sugar		

### 3.2. $^{13}\text{C}\{^{15}\text{N}\}$ REDOR enables spectral selection and quantification of carbon pools

To determine the amount of sugar relative to protein and other biomolecular contributions in the *V. cholerae* ECM, we sought to spectroscopically separate protein and polysaccharide contributions by virtue of their distinct carbon pools. Proteins contain amino acids with  $\alpha$ -carbons and carbonyls that are directly bonded to nitrogen. VPS is also known to include several modifications containing C–N pairs, including glycine and both N- and O-acetyl groups. Thus, we anticipated that carbonyl and glycine peaks could not be uniquely attributed to protein.

To begin to quantify the relative contribution of proteins to the ECM, we employed  $^{13}\text{C}\{^{15}\text{N}\}$ REDOR with 1.6 ms dephasing to select directly bonded  $^{13}\text{C}$ – $^{15}\text{N}$  pairs (Fig. 3). REDOR experiments are done in two parts: one spectrum is collected with rotor-synchronized dephasing pulses (S), and a second spectrum is collected without dephasing pulses and provides the full echo spectrum ( $S_0$ ) [33]. The difference of the two yields the REDOR difference spectrum ( $\Delta S$ ). The carbonyl peak accounts for 16% of the carbon contributions to the  $^{13}\text{C}$  CPMAS spectrum, and exhibited 76% dephasing in the one-bond  $^{13}\text{C}\{^{15}\text{N}\}$ REDOR measurement. Thus, at most, 76% of all carbonyl carbons are directly bonded to nitrogen. This represents an upper limit as some partial dephasing can result from carbons more than one-bond away from nitrogen. Carbonyl–nitrogen pairs arise from peptide bonds in proteins as well as in the glycine and N-acetyl modifications of the VPS. Glycine  $\alpha$ -carbons appear near 38 ppm, while other  $\alpha$ -carbons contribute to peak intensity at 51 and 58 ppm, although not uniquely as other carbons in cellular systems exhibit chemical shifts in this range. For example, the C2 carbon of chitosan and of N-acetylglucosamines in bacterial peptidoglycan, each with an attached nitrogen, appears between 55 and 60 ppm [34,35]. The peak integrals from the 51 and 58 ppm contributions account for 14% of the total  $^{13}\text{C}$  CPMAS spectral area (Fig. 2), and we discovered that the peak at 51 ppm exhibited 99% dephasing and the peak at 58 ppm exhibited just 17% dephasing. Thus, we can place an upper limit on the carbon mass that can be attributed to  $\alpha$ -carbons as 6% (99% of 4% plus 17% of 10%).

The above determinations considered the nineteen amino acids other than glycine. In the  $^{13}\text{C}$  spectrum, the broad region from 38 to 43 ppm contains, in part, glycine  $\alpha$ -carbons.  $^{13}\text{C}\{^{15}\text{N}\}$ REDOR identified two chemical shifts in this region that are dephased after 1.6 ms by nitrogen. The percent dephasing of the 38-ppm contribution ( $\Delta S$  peak area divided by the entire 36–43 ppm full-echo area) is 21% and for the peak at 43 ppm is 14%. Together, these data provide an accounting of glycine in the ECM: glycine  $\alpha$ -carbons account for no more than 4% of the total carbon in the ECM. Based on the maximum 6% carbon mass that can be ascribed to all other  $\alpha$ -carbons, we expected up to 0.6% dephasing corresponding to glycine  $\alpha$ -carbons in proteins (if up to 10% of the protein amino acids were glycine). The additional dephasing can be attributed to glycines associated with polysaccharide and lipid modifications. Thus, even without the prior knowledge that VPS contains glycine from previous studies of soluble parts, we can directly detect the specific prevalence of glycine far exceeding levels consistent with incorporation in proteins in the intact ECM.

$^{13}\text{C}$  peaks from 10 to 25 ppm include contributions from methyl groups that can be present in amino acids such as alanine, in lipid tails, and in N-acetylated modifications (20 ppm). The extent to which carbons were within a radius of  $\sim 2.4$  Å to a nitrogen was examined with  $^{13}\text{C}\{^{15}\text{N}\}$ REDOR with an evolution time of 8.95 ms. The peak centered at 20-ppm accounts for 13% of the total carbon pool, and was dephased by 49% (Figure S2). Thus, the methyl carbons that are proximate to  $^{15}\text{N}$  represent approximately 7% of the carbon pool by mass. Contributions to the 20-ppm peak that are not dephased by nitrogen could include O-acetyl group modifications to the VPS.

### 3.3. $^{13}\text{C}$ , $^{15}\text{N}$ , and $^{31}\text{P}$ couplings highlight lipid pools in the ECM

To characterize the remaining components of the  $^{13}\text{C}$  CPMAS spectrum, we performed additional  $^{15}\text{N}$  and  $^{31}\text{P}$  NMR experiments. We hypothesized that unidentified portions of the  $^{13}\text{C}$  intensities at 20 ppm, 38 ppm, 58 ppm, and 171 ppm could be attributed to phospholipids predicted to be present in *V. cholerae* ECM. The  $^{15}\text{N}$  CPMAS spectrum of *V. cholerae* ECM contains two prominent signals centered at 117 ppm and 33 ppm, encompassing 68% and

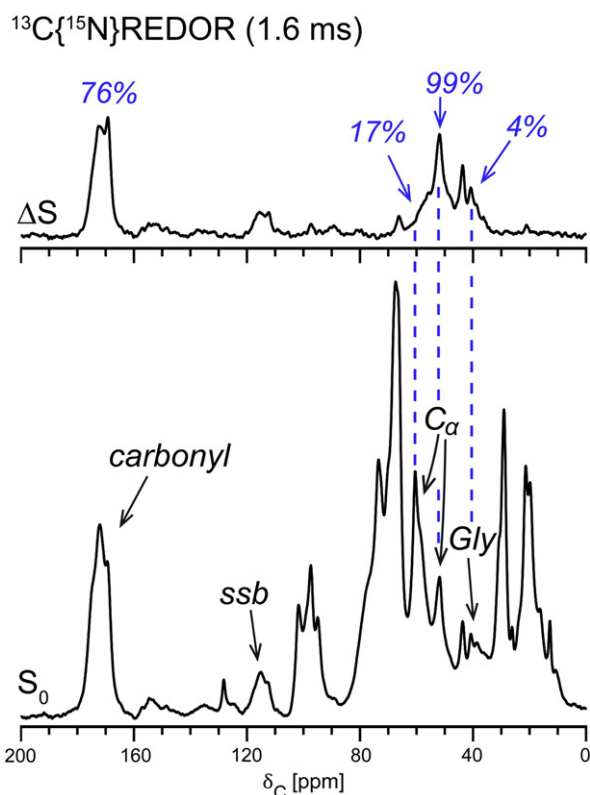


**Fig. 3.** Spectroscopic selection of one-bond C–N pairs.  $^{13}\text{C}\{^{15}\text{N}\}$ REDOR with a 1.6-ms evolution time selected for single bond pairs, including the  $\alpha$ -carbons near 40, 51, and 57 ppm (12,400 scans for both  $S_0$  and S).

23% of the total integrated spectral area, respectively (Fig. 4, Supplemental Fig. 3). The peak centered at 117 ppm corresponds to amides, as present in all peptides, some amino acid sidechains, and modifications to sugars and lipids. The  $^{15}\text{N}$  peak at 33 ppm corresponds to amines, which are present in the sidechain of lysine and commonly present near the head groups of phospholipids. The  $^{15}\text{N}$  spectrum suggests that there may also be nucleic acids in the ECM, contributing to chemical shifts near 75–80 ppm and 145–160 ppm, although they constitute less than 10% of the total nitrogen in the sample (Figure S3). Frequency-selective  $^{13}\text{C}\{^{15}\text{N}\}$ REDOR (not shown) indicated that the 117-ppm amide peak

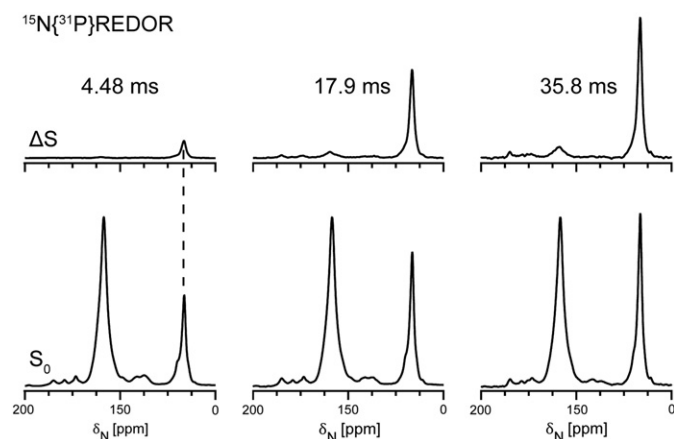


**Fig. 4.** Nitrogen pools by CPMAS and REDOR. The  $^{15}\text{N}$  full-echo ( $S_0$ ) spectrum contains two dominant peaks centered at 33 ppm and 117 ppm that together account for 92% of total spectral area (2340 scans for each  $S_0$  and S). Only the 33-ppm  $^{15}\text{N}$  peak is dephased by  $^{31}\text{P}$ , identifying nitrogens that are in or near (within  $\sim 8$  Å) phospholipid headgroups.

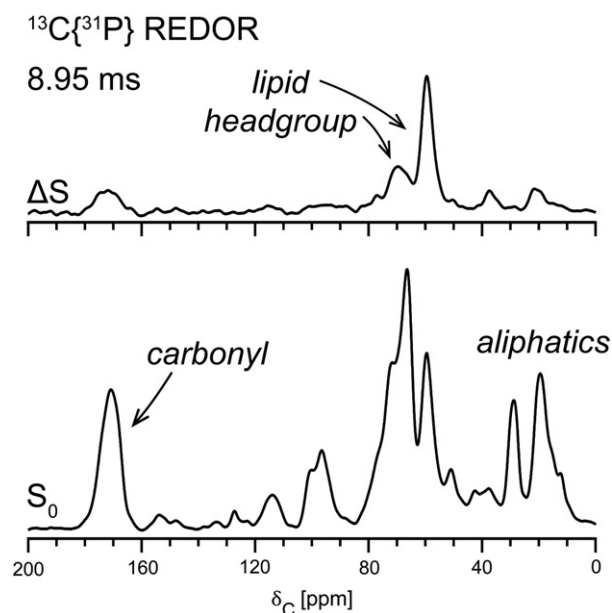


**Fig. 5.** Spectroscopic selection of carbon–phosphorous proximities.  $^{13}\text{C}\{^{31}\text{P}\}$ REDOR with 8.95 ms dephasing time was used to identify  $^{13}\text{C}$ – $^{31}\text{P}$  contacts such as those that occur in phospholipids (16,384 scans for both  $S_0$  and S).

was almost exclusively responsible for the observed dephasing in the standard  $^{13}\text{C}\{^{15}\text{N}\}$ REDOR experiment shown in Fig. 3, consistent with all the carbon–nitrogen pairs ascribed to peptides and molecular modifications as described above. The 33-ppm amine peak is much larger with respect to the amide peak than is found in typical proteins or cellular assemblies and we hypothesized that much of this might be due to specific phospholipid headgroup types or to glycine-modified lipid A that was recently discovered to contribute to LPS modifications in *V. cholerae* [36]. To determine if the nitrogen peak at 33 ppm was near to phosphorus, we performed  $^{15}\text{N}\{^{31}\text{P}\}$ REDOR for evolution times ranging from 4.48 ms to 35.8 ms. The 33-ppm  $^{15}\text{N}$  peak was dephased significantly by  $^{31}\text{P}$  and the dephasing exhibited a plateau of 81%, which suggests that the remaining 19% of the amines are not near phosphorus and could arise from lysine side chains, glycine modifications, or other amines farther than 8 Å from  $^{31}\text{P}$ .

To determine the possible carbon contributions to phospholipid, we performed  $^{13}\text{C}\{^{31}\text{P}\}$ REDOR with 8.95 ms dephasing (Fig. 5). Interestingly, the REDOR difference spectrum  $\Delta S$  contains contributions that encompassed many of the previously unidentified portions of the  $^{13}\text{C}$  CPMAS spectrum, including difference peaks at 171 ppm, 58 ppm, 38 ppm, and 20 ppm as well as at 70 ppm. The  $\Delta S$  contributions at 171 ppm can be attributed to lipid carbonyls, and peaks at 38 and 20 ppm are consistent with the shifts of lipid aliphatics and also protein aliphatics. Based on chemical shift and the strong degree to which the carbons at these chemical shifts were dephased by  $^{31}\text{P}$ , the peaks at 58 and 70 ppm correspond to carbons that are proximate to lipid headgroups [37]. The 28-ppm carbon peak was not strongly dephased by  $^{31}\text{P}$ , consistent with most  $\text{CH}_2$ s in the long-chain portion of the lipid being more than 8 Å away from  $^{31}\text{P}$ .

#### 4. Conclusions

Important genetic and molecular requirements have been identified for *V. cholerae* biofilm formation, yet a compositional accounting of these parts in the ECM has not been described. We previously defined the composition of intact ECM from the amyloid-integrated biofilms formed by uropathogenic *E. coli* [19]. An exact chemical and molecular

## ECM Carbon Pools

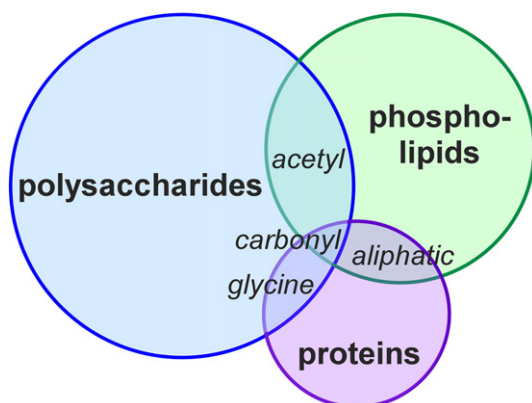


**Fig. 6.** Molecular carbon pools. Using solid-state NMR, we accounted for the molecular building blocks that make up the intact *V. cholerae* ECM. These can be considered in terms of the overall molecular mixture containing polysaccharides, phospholipids, and proteins, in which there can be complex modifications to the lipid and polysaccharide components such that building blocks including carbonyls and glycine groups can be found in multiple molecular pools.

compositional determination was possible due to the availability of samples of isolated matrix components, allowing simple carbon spectral sums to define the ECM composition. In our work described here, we have tackled a much more challenging system for which we do not have samples corresponding to matrix parts. Thus, we designed a top-down approach using solid-state NMR to dissect the more complex *V. cholerae* carbon pools. We discovered that the *V. cholerae* ECM carbon pools could be described in atomic-level detail using CPMAS and REDOR NMR. The carbon contributions are assigned approximately to sugar carbons (58%), lipid carbons (33%), and amino acid carbons (9%). These were further annotated in terms of the types of carbons in the sample, including carbonyls, amides, glyceryl carbons, anomers, and aliphatics as summarized in Table 1. In addition,  $^{15}\text{N}$  profiling revealed a large amine pool relative to amide contributions, reflecting the prevalence of molecular modifications with free amine groups.

Thus, by using strategic solid-state NMR methods on the intact ECM, we could provide an accounting of the atomic-level carbon pools in the ECM, as represented schematically in Fig. 6. Some of the molecular components of the ECM are highly modified and can include sugars with glycine modifications or lipids with extensive polysaccharide or amino acid modifications, and thus we do not further classify the exact nature of the components as percentages of VPS versus LPS, etc. Future work with individual protein, lipid, and polysaccharide preparations to provide reference spectra can be employed to define the molecular distribution in this way. Our atomic-level compositional analysis provides a detailed accounting of the molecular building blocks that one can build from. Our top-down approach described here could be implemented immediately to examine the ECM from mutant strains that might decrease VPS production or lipid release beyond the cell surface; or to monitor changes that may accompany environmental variations and stressors such as altered nutrient composition, oxidative stress or antibiotics. Our analysis here was performed on ECM isolated from *V. cholerae* biofilms formed on a minimal agar medium and has demonstrated that solid-state NMR is a valuable tool to dissect complex biofilm systems.

## Acknowledgements

This research was supported by the NIH Director's New Innovator Award to L.C. (DP2OD007488), by the National Institutes of Health to

F.Y. (AI055987), and the Stanford Terman Fellowship (L.C.). C.R. is supported by the Althouse Stanford Graduate Fellowship. We acknowledge Dr. Ji Youn Lim for assistance with electron microscopy and we acknowledge support from the Cell Sciences Imaging Facility at Stanford for electron microscopy access and assistance.

## Appendix A. Supplementary data

Supplementary data to this article can be found online at <http://dx.doi.org/10.1016/j.bbamm.2014.05.030>.

## References

- [1] L. Hall-Stoodley, J.W. Costerton, P. Stoodley, Nat. Rev. Microbiol. 2 (2) (2004) 95–108.
- [2] R.M. Donlan, J.W. Costerton, Clin. Microbiol. Rev. 15 (2) (2002) 167–193.
- [3] J.W. Costerton, Z. Lewandowski, D.E. Caldwell, D.R. Korber, H.M. Lappin-Scott, Annu. Rev. Microbiol. 49 (1995) 35.
- [4] I.W. Sutherland, Trends Microbiol. 9 (2001) 6.
- [5] H.C. Flemming, Appl. Microbiol. Biotechnol. 59 (6) (2002) 629–640.
- [6] B. McLaughlin, Stapleton, Matheson, Dart, J. Appl. Microbiol. 84 (5) (1998) 827–838.
- [7] P.Y. Litzler, L. Benard, N. Barbier-Frebouge, S. Vilain, T. Jouenne, E. Beucher, C. Bunel, J.F. Lemeland, J.P. Bessou, The Journal of Thoracic and Cardiovascular Surgery 134 (4) (2007) 1025–1032.
- [8] G.G. Anderson, J.J. Palermo, J.D. Schilling, R. Roth, J. Heuser, S.J. Hultgren, Science 301 (5629) (2003) 105–107.
- [9] M.G. Blango, M.A. Mulvey, Antimicrob. Agents Chemother. 54 (5) (2010) 1855–1863.
- [10] L. Cegelski, J.S. Pinkner, N.D. Hammer, C.K. Cusumano, C.S. Hung, E. Chorell, V. Aberg, J.N. Walker, P.C. Seed, F. Almqvist, M.R. Chapman, S.J. Hultgren, Nat. Chem. Biol. 5 (12) (2009) 913–919.
- [11] G.G. Anderson, K.W. Dodson, T.M. Hooton, S.J. Hultgren, Trends Microbiol. 12 (9) (2004) 424–430.
- [12] P.K. Singh, A.L. Schaefer, M.R. Parsek, T.O. Moninger, M.J. Welsh, E.P. Greenberg, Nature 407 (6805) (2000) 762–764.
- [13] J.B. Kaper, J.G. Morris Jr., M.M. Levine, Clin. Microbiol. Rev. 8 (1995) 21.
- [14] M. Alam, M. Sultana, G.B. Nair, R.B. Sack, D.A. Sack, A.K. Siddique, A. Ali, A. Huq, R.R. Colwell, Appl. Environ. Microbiol. 72 (4) (2006) 2849–2855.
- [15] C. Matz, D. McDougald, A.M. Moreno, P.Y. Yung, F.H. Yildiz, S. Kjelleberg, Proc. Natl. Acad. Sci. U. S. A. 102 (46) (2005) 16819–16824.
- [16] S.M. Faruque, M.J. Albert, J.J. Mekalanos, Microbiol. Mol. Biol. Rev. 62 (4) (1998) 14.
- [17] S.M. Faruque, K. Biswas, S.M. Udden, Q.S. Ahmad, D.A. Sack, G.B. Nair, J.J. Mekalanos, Proc. Natl. Acad. Sci. U. S. A. 103 (16) (2006) 6350–6355.
- [18] I. Sutherland, Microbiology 147 (2001) 7.
- [19] O.A. McCrate, X. Zhou, C. Reichhardt, L. Cegelski, J. Mol. Biol. 425 (2013) 4286–4294.
- [20] C. Reichhardt, L. Cegelski, Mol. Phys. 112 (7) (2013) 887–894.
- [21] S.J. Kim, L. Cegelski, D. Stueber, M. Singh, E. Dietrich, K.S.E. Tanaka, T.R. Parr, A.R. Far, J. Schaefer, J. Mol. Biol. 377 (1) (2008) 281–293.
- [22] L. Cegelski, S.J. Kim, A.W. Hing, D. Studelska, R. O'Connor, A. Mehta, J. Schaefer, Biophys. J. 82 (1) (2002) 468A–468A.
- [23] J. Schaefer, K.J. Kramer, J.R. Garbow, G.S. Jacob, E.O. Stejskal, T.L. Hopkins, R.D. Speirs, Science 235 (4793) (1987) 1200–1204.
- [24] L. Cegelski, J. Schaefer, J. Biol. Chem. 280 (47) (2005) 39238–39245.
- [25] F.H. Yildiz, G.K. Schoolnik, Microbiology 96 (1999) 15.
- [26] J.C. Fong, K.A. Syed, K.E. Klose, F.H. Yildiz, Microbiology 156 (Pt 9) (2010) 2757–2769.
- [27] F. Yildiz, J. Fong, I. Sadovskaya, T. Grard, E. Vinogradov, PLoS One 9 (1) (2014).
- [28] V. Berk, J.C.N. Fong, G.T. Dempsey, O.N. Develiglu, X.W. Zhuang, J. Liphardt, F.H. Yildiz, S. Chu, Science 337 (6091) (2012) 236–239.
- [29] M. Duperthuy, A.E. Sjöström, D. Sabharwal, F. Damghani, B.E. Uhlin, S.N. Wai, PLoS Pathog. 9 (10) (2013) e1003620.
- [30] E. Altindis, Y. Fu, J.J. Mekalanos, Proc. Natl. Acad. Sci. (2014).
- [31] D.R. Leitner, S. Feichter, K. Schild-Prufert, G.N. Rechberger, J. Reidl, S. Schild, Infect. Immun. 81 (7) (2013) 15.
- [32] J. Schaefer, E.O. Stejskal, R. Buchdahl, Macromolecules 8 (3) (1975) 6.
- [33] T. Gullion, J. Schaefer, Journal of Magnetic Resonance 81 (1) (1969) 196–200 (1989).
- [34] A.B.V. Kumar, L.R. Gowda, R.N. Tharanathan, Eur. J. Biochem. 271 (4) (2004) 713–723.
- [35] T. Kern, S. Hediger, P. Muller, C. Giustini, B. Joris, C. Bougault, W. Vollmer, J.P. Simorre, J. Am. Chem. Soc. 130 (17) (2008) 5618.
- [36] J.V. Hankins, J.A. Madsen, D.K. Giles, J.S. Brodbelt, M.S. Trent, Proc. Natl. Acad. Sci. (2012).
- [37] L. Cegelski, C.V. Rice, R.D. O'Connor, A.L. Caruano, G.P. Tochtrop, Z.Y. Cai, D.F. Covey, J. Schaefer, Drug Dev. Res. 66 (2) (2005) 93–102.